doi:10.1016/j.jmb.2010.09.022 J. Mol. Biol. (2010) 403, 616–629

Contents lists available at www.sciencedirect.com

Journal of Molecular Biology

journal homepage: http://ees.elsevier.com.jmb

Structure-Based Analysis of *Toxoplasma gondii* Profilin: A Parasite-Specific Motif Is Required for Recognition by Toll-Like Receptor 11

Kaury Kucera[1], A. Alicia Koblansky[2], Lauren P. Saunders[1], Kendra B. Frederick[1], Enrique M. De La Cruz[1], Sankar Ghosh[2] and Yorgo Modis[1]*

[1]*Department of Molecular Biophysics and Biochemistry, Yale University, 266 Whitney Avenue, New Haven, CT 06520, USA*
[2]*Department of Microbiology and Immunology, College of Physicians and Surgeons, Columbia University, 701 West 168 Street, New York, NY 10032, USA*

Received 9 June 2010; received in revised form 2 September 2010; accepted 8 September 2010
Available online 17 September 2010

Edited by I. Wilson

Keywords:
Toxoplasma gondii; profilin; Toll-like receptor 11; innate immune recognition; actin binding

Profilins promote actin polymerization by exchanging ADP for ATP on monomeric actin and delivering ATP-actin to growing filament barbed ends. Apicomplexan protozoa such as *Toxoplasma gondii* invade host cells using an actin-dependent gliding motility. Toll-like receptor (TLR) 11 generates an innate immune response upon sensing *T. gondii* profilin (TgPRF). The crystal structure of TgPRF reveals a parasite-specific surface motif consisting of an acidic loop, followed by a long β-hairpin. A series of structure-based profilin mutants show that TLR11 recognition of the acidic loop is responsible for most of the interleukin (IL)-12 secretion response to TgPRF in peritoneal macrophages. Deletion of both the acidic loop and the β-hairpin completely abrogates IL-12 secretion. Insertion of the *T. gondii* acidic loop and β-hairpin into yeast profilin is sufficient to generate TLR11-dependent signaling. Substitution of the acidic loop in TgPRF with the homologous loop from the apicomplexan parasite *Cryptosporidium parvum* does not affect TLR11-dependent IL-12 secretion, while substitution with the acidic loop from *Plasmodium falciparum* results in reduced but significant IL-12 secretion. We conclude that the parasite-specific motif in TgPRF is the key molecular pattern recognized by TLR11. Unlike other profilins, TgPRF slows nucleotide exchange on monomeric rabbit actin and binds rabbit actin weakly. The putative TgPRF actin-binding surface includes the β-hairpin and diverges widely from the actin-binding surfaces of vertebrate profilins.

*Corresponding author. E-mail address: yorgo.modis@yale.edu.

Abbreviations used: TLR, Toll-like receptor; TgPRF, *Toxoplasma gondii* profilin; IL, interleukin; G-actin, globular actin; ADF, actin-depolymerizing factor; PfPRF, *Plasmodium falciparum* profilin; ScPRF, *S. cerevisiae* profilin; TgFRM2, *Toxoplasma gondii* formin 2; ITC, isothermal titration calorimetry; PIP2, phosphatidylinositol 4,5-bisphosphate; PBS, phosphate-buffered saline; PDB, Protein Data Bank.

Introduction

The ancient phylum of Apicomplexa encompasses thousands of unicellular animal parasite species, including important human pathogens such as *Plasmodium*, *Toxoplasma*, *Cryptosporidia*, and *Cyclospora* species. In the United States, *Toxoplasma gondii* infects nearly a quarter of the population and is the third leading cause of death attributed to food-borne

illness. While most healthy adults do not develop disease symptoms, congenital infection of infants during pregnancy can lead to severe developmental impairments or death. Toxoplasmosis can also be fatal in immunocompromised patients.[1]

T. gondii and other apicomplexan parasites rely on changes in the actin cytoskeleton, especially at the apical end, to invade the host cell. Specifically, host-cell invasion requires parasite gliding motility,[2] which is powered by the movement of TgMyoA and possibly other myosin motors along unusually short and unstable actin filaments.[3–7] One actin and 10 putative actin-related genes have been identified or annotated in the *T. gondii* genome.[8,9] The profilin from *T. gondii* (TgPRF) is strictly required for the actin-dependent gliding motility that enables *T. gondii* to invade and exit from host cells.[10] Because of the low abundance of actin filaments, apicomplexans depend on proteins governing actin dynamics, and they are extremely susceptible to compounds that modulate actin polymerization or depolymerization.[11–14]

In most eukaryotes, a profilin promotes the rapid elongation of actin filaments by delivering monomeric (globular) actin, or G-actin, to the filament barbed ends.[10,15,16] Apicomplexans lacking profilin can grow and replicate, but they can cannot invade host cells, presumably because their ability to polymerize actin for host invasion is compromised.[10] Profilin is recruited to the barbed end when it binds to proline-rich regions on a formin protein, which is bound to the barbed end of most growing actin filaments. Binding of multiple profilin–actin complexes to formin concentrates actin near the barbed end, thereby stimulating elongation of the filament. Yeast and human profilins catalyze the exchange of actin-bound ADP for cytosolic ATP.[15] Interestingly, one of the two actin-depolymerizing factor (ADF) homologues of *Plasmodium falciparum*, PfADF1, slightly enhances nucleotide exchange on G-actin,[17] in contrast to the typical inhibition of nucleotide exchange caused by ADFs.[18,19] However, the single ADF of *T. gondii*, TgADF, inhibits nucleotide exchange on both *T. gondii* actin and rabbit G-actin and was recently shown to have weak severing activity on *T. gondii* actin.[20] Thus, the primary function of TgADF appears to promote efficient turnover of actin filaments by sequestering actin monomers.

Apicomplexans lack the Arp2/3 complex, an important nucleator of actin filaments in other phyla.[9] However, apicomplexan genomes encode other putative actin regulatory proteins including barbed-end capping factors, G-actin-sequestering factors, formins, and cofilin-like proteins that may promote actin depolymerization.[21,22] The regulatory activities of most of these proteins on filamentous actin have yet to be demonstrated experimentally.[20]

Some profilins are known to bind inositide lipid head groups, providing a possible mechanism for the localization of profilins to actin-rich regions near the plasma membrane.[23,24] Phosphatidylinositides may also compete with the profilin–actin interaction, promoting the release of actin near the membrane.[15] It has been proposed that profilin regulates the cleavage of phosphatidylinositide head groups and thereby link cytoskeletal dynamics to phosphoinositide metabolism.[25–28]

Toll-like receptors (TLRs) are responsible for the initial recognition of a wide variety of molecular patterns that are highly conserved in microbes but absent in the host.[29] TLR11 generates a powerful NF-κB-dependent inflammatory response upon recognizing TgPRF. TLR11-deficient mice have a greatly impaired interleukin (IL)-12 response when challenged with *T. gondii*,[30] and *T. gondii* parasites lacking profilin are unable to induce TLR11-dependent production of the defensive host cytokine IL-12.[10] Profilins from other apicomplexan parasites including *P. falciparum*, *Cryptosporidium parvum*, and *Eimeria tenella* also activate TLR11-dependent signaling but to a lesser extent than TgPRF.[30,31] Following the same paradigm as all known TLR ligands, apicomplexan profilins have conserved features that are not found in other eukaryotic profilins. However, the molecular basis for the recognition of TgPRF by TLR11 remains unknown.

We report here a structure-based analysis of the molecular basis of the recognition of TgPRF by TLR11. The structure shows broad similarities to *P. falciparum* profilin (PfPRF).[32] However, the structure of TgPRF reveals specific surface features that are likely candidates for TLR11 recognition of *T. gondii*. By mutating these features, we show that the parasite-specific motif consisting of an acidic loop and a β-hairpin is important for TLR11 recognition, while the putative actin-binding surface is not. By inserting this motif from *T. gondii* into yeast profilin, we show that the motif is sufficient to generate TLR11-dependent signaling. We have therefore identified the molecular pattern that is recognized by TLR11. Other mutants show that the acidic loop performs a major function in TLR11-dependent recognition of apicomplexan profilins. The structure of TgPRF also provides a framework for understanding its low actin polymerization activity[10] and its contribution to the unusually short length and high depolymerization rates of apicomplexan actin filaments.

Results

Overall architecture of TgPRF

TgPRF adopts the overall canonical profilin fold and exists as a monomer in solution as evidenced by size-exclusion chromatography and multi-angle laser light scattering (data not shown). TgPRF has N- and

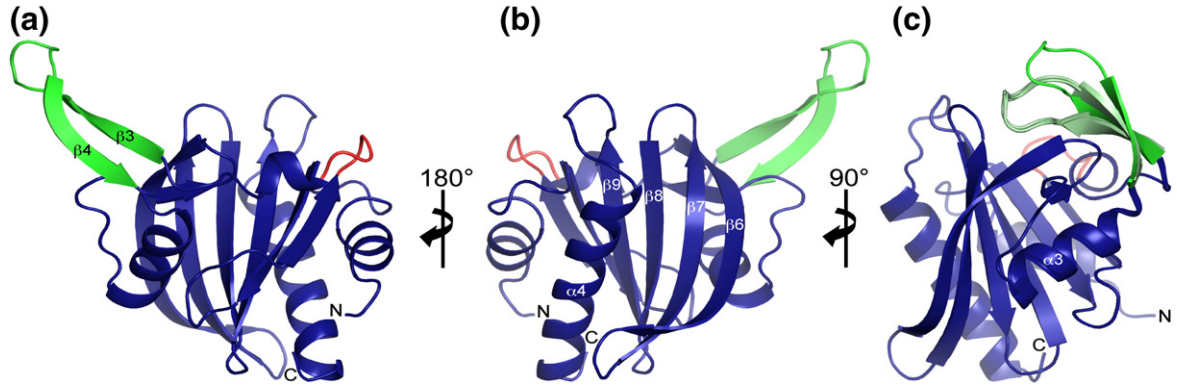

Fig. 1. Overall structure of TgPRF. (a–c) Ribbon representations of TgPRF in blue with the acidic loop and β-hairpin highlighted in red and green, respectively. (b) TgPRF is in the standard profilin orientation, which shows the putative actin-binding surface. (c) An overlay of all four molecules in the asymmetric unit using residues 38–80 as the reference shows flexibility in the extended β-hairpin. β-Hairpin residues 50–67 have an average RMSD of 0.50 Å. The average main-chain RMSD between the four molecules is 0.15 Å.

C-terminal α-helices that lie parallel on one molecular face and two α-helices on the opposite face that sandwich seven antiparallel β-strands (Fig. 1a). The internal β-sheet of TgPRF shows a high degree of structural conservation to non-apicomplexan parasite profilins with the exception of elongated β-strands 6 and 7, which form the solvent-exposed edge of the β-sheet. These strands extend past the conserved non-apicomplexan parasite profilin strands 4 and 5 by seven residues, making them nearly twice as long as in other profilins.

There are notable differences in the structure of TgPRF compared to non-apicomplexan profilin structures. TgPRF has a 31-amino-acid insertion between β-strand 2 and α-helix 3 (residues 37–68), with general features that appear to be conserved in

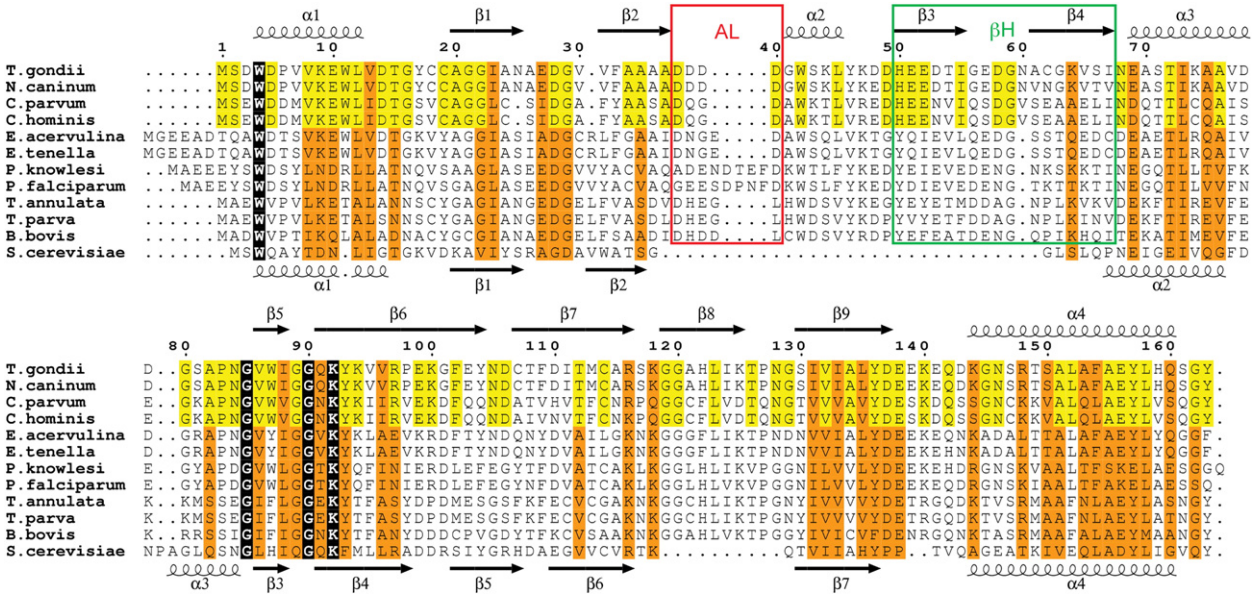

Fig. 2. Sequence alignment of apicomplexan protozoan profilins. Secondary structure is shown for TgPRF on top and for *S. cerevisiae*, representing the conserved non-apicomplexan profilin structure, on the bottom. Secondary-structure nomenclature follows the canonical profilin fold. Strictly conserved residues are highlighted in black, orange denotes conserved residues, and residues absolutely conserved in the parasites most closely related to TgPRF are in yellow. The apicomplexan-specific acidic loop (AL) and β-hairpin (βH) are boxed in red and green, respectively. GenBank accession numbers are as follows: *T. gondii*, 61612092; *C. parvum*, 126644761; *Cryptosporidium hominis*, 67593937; *Eimeria acervulina*, 405637; *E. tenella*, 117960055; *P. knowlesi*, 193808670; *P. falciparum*, 206581653; *Theileria annulata*, 84994870; *T. parva*, 71030962; *B. bovis*, 78458472; *S. cerevisiae*, 6324696. The sequence for *Neospora caninum* is from toxoDB, accession no. NC_LIV_10440.

apicomplexan parasites (Figs. 1 and 2). In TgPRF, this novel region includes a highly acidic loop, α-helix 2 (which is absent in non-apicomplexan profilins), and a prominent β-hairpin (residues 50–67) that extends away from the otherwise globular protein.

We determined the structure of TgPRF with four molecules in the asymmetric unit showing the extended β-hairpin in two distinct conformations (Fig. 1b). The average root-mean-square deviation (RMSD) of all four molecules, excluding the β-hairpin residues, is 0.15 Å. The β-hairpin structures of three of the molecules overlay well with an average RMSD of 0.25 Å. The β-hairpin of the fourth molecule, crystallized in a more extended conformation, has an average RMSD between it and the β-hairpin of the other three molecules of 0.75 Å. Normal mode analysis using both species of TgPRF predicts even greater β-hairpin flexibility than was observed in the crystallized conformations of TgPRF. Thus, we interpret the different conformations observed in the crystal to represent flexibility of the β-hairpin.

Novel structural features of TgPRF stimulate TLR11-dependent signaling

TgPRF shares low (18–24%) sequence identity to non-apicomplexan profilins. Comparing profilins from all sequenced species of apicomplexan parasites shows better conservation and suggests that apicomplexan protozoan parasites contain a divergent class of profilins (Fig. 2). TgPRF and PfPRF, the causative agent of malaria, share 42% sequence identity, suggesting that even within a subset of closely related apicomplexan parasites, structural and perhaps functional differences have evolved in their profilins. Though TgPRF and PfPRF have a main-chain RMSD of 1.06 Å (Fig. 3), direct comparison of TgPRF and PfPRF structures[32] shows that regions with divergent sequences translate to surface-exposed differences in the protein structures (Figs. 2 and 3). The outer face of the apicomplexan-specific β-hairpin, the novel acidic loop, and residues on the putative polyproline binding cleft formed by the N- and C-terminal α-helices represent the most divergent regions, while the surface corresponding to the actin-binding site of non-apicomplexan profilins is most conserved.

TgPRF and PfPRF diverge in the region preceding and including the large apicomplexan-specific β-hairpin extension (Fig. 2). TgPRF has a surface-exposed acidic loop in this region composed of four aspartic acids, followed by α-helix 2. TgPRF and PfPRF have almost identical backbone and side-chain conformations for residues flanking the acidic loop, but the loops adopt different structures (Fig. 3d). The PfPRF acidic loop contains five additional residues, forming a more prominent but less acidic surface feature. In addition to the acidic loop differences, TgPRF has one extra residue in the extended β-hairpin compared to PfPRF. Notably, TgPRF has a solvent-exposed cysteine on one strand of the extended β-hairpin that is not present in PfPRF.

To test whether the novel structural features of TgPRF are recognized by TLR11, we created various mutants of TgPRF. First, we replaced the acidic loop and flanking residues (36–44) with two glycines, which correspond to the homologous sequence in both *Saccharomyces cerevisiae* and mouse profilins (mutant ΔAL). Second, we deleted the β-hairpin (residues 50–67, mutant ΔBH). In a third mutant, both the acidic loop and the β-hairpin were deleted (ΔALBH). Finally, to test the importance of the β-hairpin, we mutated the β-hairpin residues to the homologous sequence in PfPRF. All profilin mutants were tested for the ability to stimulate IL-12(p40) in peritoneal macrophages isolated from wild-type mice and mice lacking TLR11 ($TLR11^{-/-}$). Importantly, deletion of the acidic loop reduced IL-12 production in wild-type cells by at least 70% relative to wild-type TgPRF, while changing the amino acid sequence or deletion of the β-hairpin did not significantly reduce IL-12 production. However, stimulation with the mutant lacking both the acidic loop and the β-hairpin failed to induce significant IL-12 production (Fig. 4b), suggesting that the acidic loop/β-hairpin motif is required for TLR11 recognition.

To test whether the acidic loop/β-hairpin motif is sufficient for TLR11 recognition, we inserted the acidic loop and/or β-hairpin from TgPRF into *S. cerevisiae* profilin (ScPRF). We found that insertion of either the acidic loop or the β-hairpin from TgPRF into the yeast profilin induced low levels of IL-12 production, while insertion of both the acidic loop and the β-hairpin induced nearly the same level of IL-12 production as for wild-type TgPRF (Fig. 4c). Wild-type ScPRF did not induce significant levels of IL-12 production. A peptide consisting of the 35 C-terminal amino acids of *Legionella* flagellin has been shown to elicit signaling by cytosolic innate immune receptor Ipaf, which senses bacterial flagellin.[33] Similarly, we used a synthetic peptide with the acidic loop and β-hairpin sequence (ALBH peptide) to test whether the peptide alone is sufficient for TLR11 recognition. The ALBH peptide did not stimulate IL-12 production (Fig. 4b), indicating that the physical constraints imposed by the context of the TgPRF three-dimensional fold are required to effectively present the β-hairpin for TLR11 recognition.

For a finer analysis of the role of the acidic loop in TLR11 recognition, we substituted the acidic loop of TgPRF with the homologous acidic loops from the apicomplexan parasites *C. parvum* and *P. falciparum*. The *C. parvum* acidic loop differs from that of *T. gondii* by only two amino acids; thus, substitution with the *C. parvum* acidic loop is equivalent to a D38Q, D39G double point mutation of TgPRF. This mutant induced the same level of IL-12 production

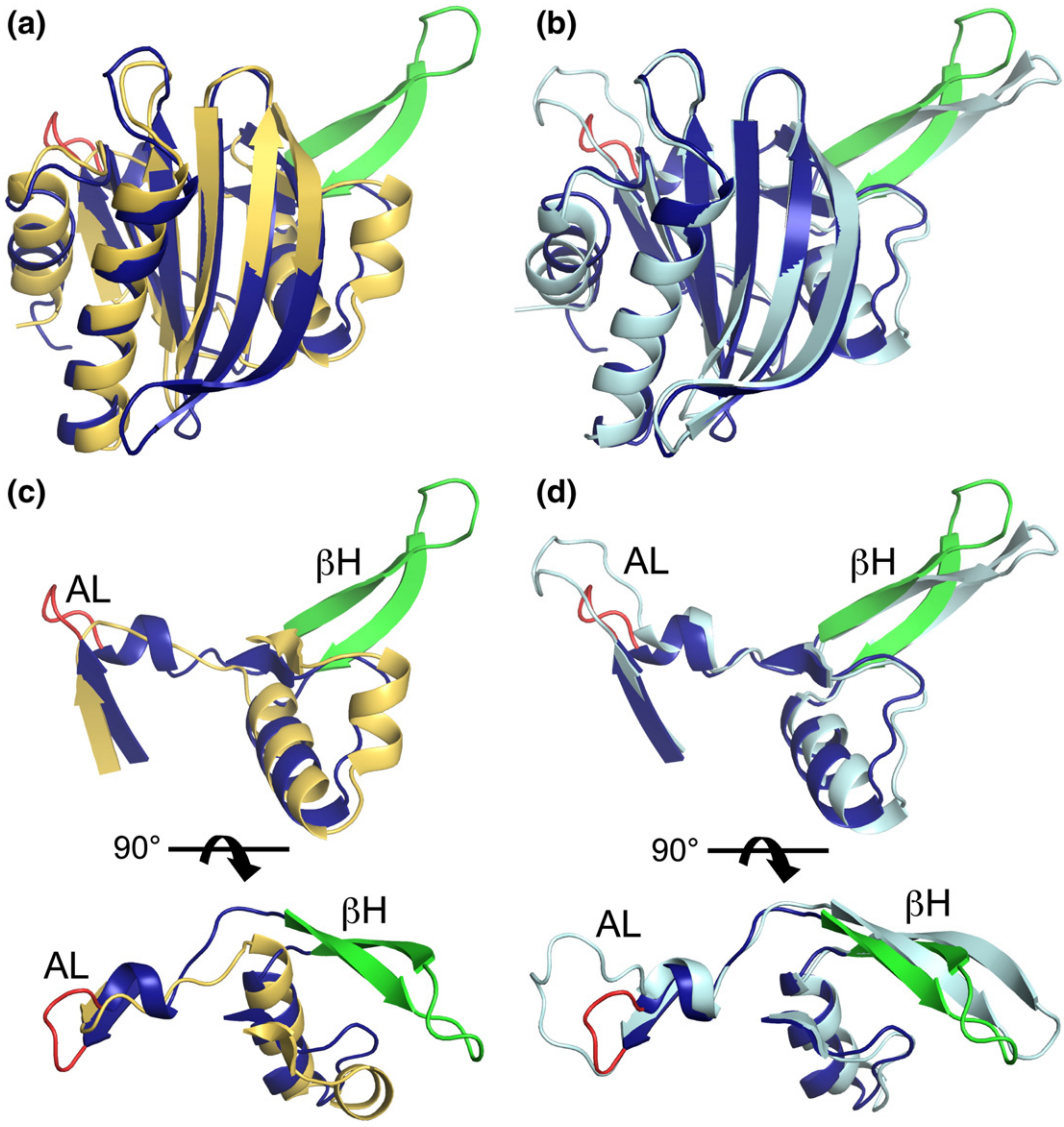

Fig. 3. Structural comparison of profilins from *T. gondii*, *S. cerevisiae*, and *P. falciparum*. TgPRF is in blue with red acidic loop and green β-hairpin. (a) Superposition of TgPRF onto ScPRF (PDB ID: 1YPR) in orange, which represents the conserved non-apicomplexan profilin structure (RMSD is 2.35 Å). (b) Superposition of TgPRF onto PfPRF (PDB ID: 2JKF) in cyan (RMSD is 1.06 Å). (c and d) The divergent features of TgPRF include a highly acidic loop (AL, TgPRF residues 37–40) and a β-hairpin (βH, residues 50–67). The latter is conserved among apicomplexans in length and overall structure but not in sequence.

as wild-type TgPRF (Fig. 4d). Substitution of the longer acidic loop of *P. falciparum* (Fig. 2) into TgPRF resulted in lower but significant IL-12 production (Fig. 4d). IL-12 production was significantly reduced only when the acidic loop is replaced with two glycines, which corresponds to the homologous residues in *S. cerevisiae* and mouse profilin.

To test whether amino acids on the putative actin-binding surface of TgPRF are recognized by TLR11, we created two additional mutants in which we replaced two or six unconserved side chains on the actin-binding surface with their structural homologues from *Schizosaccharomyces pombe* and bovine profilin: R97N and P98I; K94Q, V95F, R97N, P98I, T112A, and M113T.[16,34] Both of these mutants showed a 10% reduction in IL-12 production relative to wild-type TgPRF, which is unlikely to be significant (Fig. 4b).

All profilin mutants eluted from a size-exclusion chromatography column as single monomeric peaks at their expected sizes (data not shown). Circular dichroism (CD) spectra confirmed that wild-type TgPRF, ScPRF, and all profilin mutants and chimeras had similar secondary structure (Fig. S1). Moreover, CD measurements during reversible thermal denaturation showed that, although the

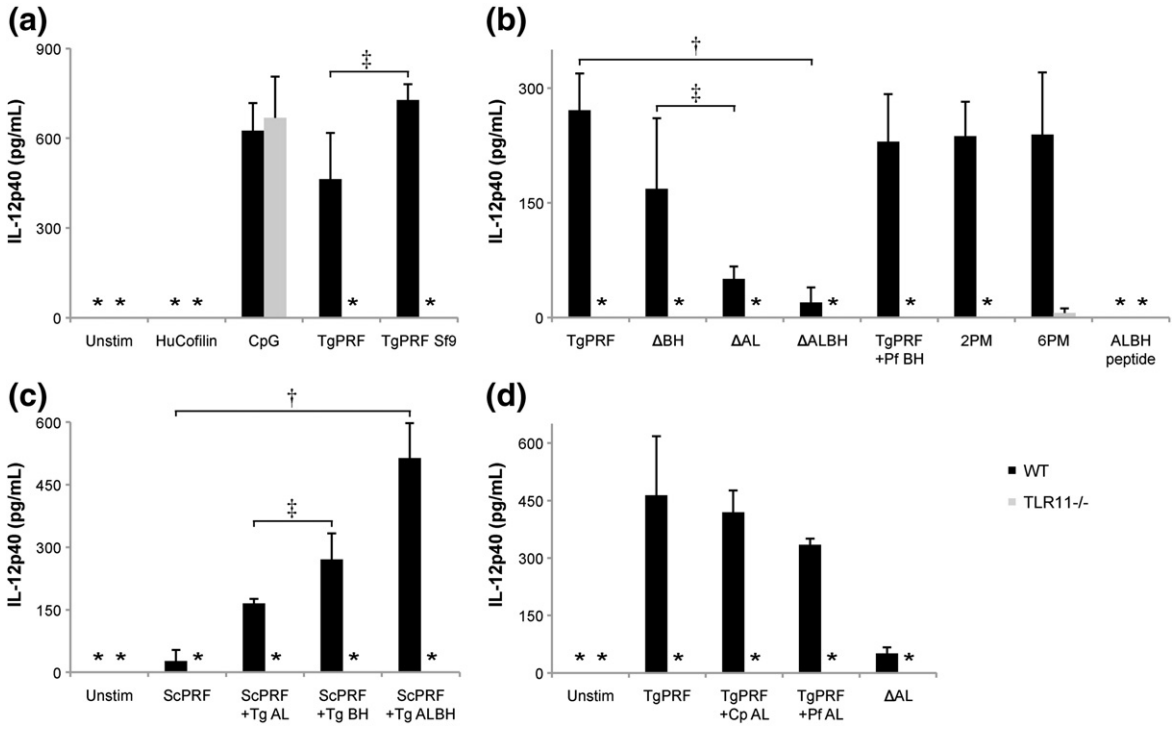

Fig. 4. TLR11 recognizes specific features of TgPRF. (a) Peritoneal macrophages from wild-type (WT) and TLR11$^{-/-}$ mice were stimulated for 24 h with 3.0 μg/ml of TgPRF, TgPRF purified from Sf9 insect cells, or 5 mM CpG as a positive control. Macrophages were stimulated with 3.0 μg/ml of human cofilin as a negative control. (b) Peritoneal macrophages were stimulated with 3.0 μg/ml of TgPRF, acidic loop deletion mutant TgPRF (ΔAL), β-hairpin deletion mutant TgPRF (ΔBH), double deletion mutant TgPRF (ΔALBH), a TgPRF mutant with *P. falciparum* β-hairpin (TgPRF+Pf BH), actin-binding surface TgPRF point mutants 2 PM or 6 PM, and a peptide with the acidic loop and β-hairpin sequence (ALBH peptide). (c) Peritoneal macrophages were stimulated with TgPRF, a TgPRF mutant with the acidic loop from *C. parvum* (TgPRF +Cp AL), a TgPRF mutant with the acidic loop from *P. falciparum* (TgPRF +Pf AL), and a TgPRF acidic loop deletion mutant that, like ScPRF, has two glycines in place of the acidic loop (TgPRF +Sc AL). (d) Peritoneal macrophages were stimulated with ScPRF, an ScPRF mutant containing the *T. gondii* acidic loop (ScPRF +Tg AL), an ScPRF mutant containing the *T. gondii* β-hairpin (ScPRF +Tg BH), and an ScPRF mutant containing both the acidic loop and the β-hairpin (ScPRF +Tg ALBH). After 24 h, supernatant was removed and analyzed for IL-12p40 levels by ELISA. Each bar represents the mean ±SD of triplicate measurements of three independent experiments. Statistical analysis was performed using the Student's *t* test where $^{\dagger}P<0.01$ and $^{\ddagger}P>0.05$ arbitrary units. In the columns marked with an asterisk, the IL-12p40 concentration was below detectable levels. Together, these data show that the parasite-specific motif in TgPRF is the key determinant for recognition by TLR11, with the acidic loop as the primary determinant and the β-hairpin as a secondary but necessary determinant.

melting temperature varied between mutants, each mutant remained fully folded well above 25 °C, the temperature at which the signaling assays were performed (Table 1).

TLR11$^{-/-}$ macrophages failed to produce significant levels of IL-12 when stimulated with any of our profilin constructs, although other TLR ligands such as lipopolysaccharide (data not shown) and unmethylated CpG DNA oligonucleotides did stimulate IL-12 production in these cells (Fig. 4a). This is consistent with previous studies suggesting that TLR11 can recognize TgPRF.[30] TgPRF purified from insect cells stimulated similar levels of TLR11 IL-12 production as TgPRF from *Escherichia coli* (Fig. 4a), indicating that our measurements are not significantly influenced by bacterial contaminants such as lipopolysaccharide. Together, these data suggest that the acidic loop and β-hairpin are key molecular patterns that are recognized by TLR11.

Surface and actin-binding properties of TgPRF

Like all profilin structures determined to date, TgPRF has N- and C-terminal α-helices, 1 and 4, that lie parallel on one face of the protein. Three co-crystal structures of proline-rich peptides with human profilin 1, mouse profilin 2a, and PfPRF show that four or five aromatic residues near the helix 1–helix 4 interface bind directly to the peptides.[32,35,36] The unliganded bovine and yeast

Table 1. Summary of profilin mutants and analysis of wild-type and mutant TgPRF constructs based on CD measurements

Protein	Mutated amino acids	T_m (°C)
TgPRF	Wild-type *T. gondii* sequence	53.1
ΔAL	Amino acids 36–44 replaced with GG	44.0
ΔBH	Amino acids 50–67 deleted	54.3
ΔALBH	Amino acids 36–67 replaced with GG	50.1
TgPRF +Pf BH	Amino acids 50–67 replaced with PfPRF amino acids 59–74	59.5
TgPRF +Cp AL	D38Q, D39G	51.3
TgPRF +Pf AL	Amino acids 37–41 replaced with PfPRF amino acids 40–50	42.5
2 PM	R97N, P98I	—
6 PM	K94Q, V95F, R97N, P98I, T112A, M113T	62.2
ALBH peptide	Consists of TgPRF amino acids 36–67 only	N.A.
ScPRF	Wild-type *S. cerevisiae* sequence	67.9
ScPRF +Tg AL	TgPRF amino acids 37–40 inserted after ScPRF amino acid 33	45.9
ScPRF +Tg BH	TgPRF amino acids 50–67 inserted after ScPRF amino acid 39	36.7
ScPRF +Tg ALBH	TgPRF amino acids 37–40 and 50–67 inserted after ScPRF amino acids 33 and 39, respectively	>95.0

profilin structures have aromatic residues in all five positions, and yeast mutagenesis studies show that these residues directly interact with polyproline.[37] In TgPRF, four of the five aromatic residues, W4, F32, Y157, and Y163, are conserved and have the same relative orientations as in canonical profilins. An otherwise conserved tyrosine (Y5 in yeast sequences) is missing in TgPRF; however, TgPRF contains an additional aromatic residue nearby (W11), pointed at the polyproline binding cleft. Interestingly, PfPRF has a different unconserved aromatic residue, Y5, which binds polyproline directly.[32] While the array of conserved aromatic residues in the helix 1–helix 4 interface of TgPRF suggests that TgPRF should bind polyproline, we were unable to detect any binding of TgPRF to a proline-rich peptide from the *T. gondii* formin 2 (TgFRM2) FH1 domain (MPPPPPPGLTP) by isothermal titration calorimetry (ITC). Moreover, a structure of TgPRF determined from crystals grown in the presence of 2.8 mM TgFRM2-FH1 peptide did not reveal any electron density corresponding to the peptide (data not shown).

TgPRF is indispensible for parasite viability and pathogenesis but the specific cellular functions of apicomplexan parasite profilins are not well understood. TgPRF may regulate actin polymerization in parasites, though little is known about protozoan parasite actin or actin regulation. One conserved function of profilins is the ability to increase nucleotide exchange in monomeric actin. Though previous studies have demonstrated that apicomplexan profilins bind vertebrate actin *in vitro*,[32] their nucleotide exchange activity has not been measured.

TgPRF unexpectedly slows ATP exchange from vertebrate actin monomers (Fig. 5). The acidic loop deletion mutant and the mutant with six point mutations on the putative actin-binding surface also slow actin nucleotide exchange (Fig. 5). The β-hairpin deletion mutant binds actin monomers weakly and inhibits ATP exchange only at very high concentrations (>50 μM). Inhibition of actin ATP exchange is a well-documented activity of cofilin,[18,19] which regulates actin dynamics by severing actin filiments.[38–41] TgPRF binds vertebrate ATP-actin with a K_d of 13.9 ± 5.0 μM. This value is in reasonable agreement with the previously reported value of 6±1 μM[10] and similar to other reported apicomplexan profilin–vertebrate actin affinities,[10] but weaker than profilin–actin interactions reported for other organisms. Human cofilin binds monomeric actin with a 1.7 (±0.3) μM dissociation constant (K_d) (Fig. 5b) and *Acanthamoeba* profilin binds to amoeba actin with a K_d of 1 μM.[42] The TgPRF β-hairpin deletion mutant binds vertebrate ATP-actin weakly with a K_d >150 μM. This result is consistent with a previously proposed model of *P. falciparum* actin bound to PfPRF.[32] Though the activities of various apicomplexan actin regulatory proteins have been studied using vertebrate actin,[17,22] future studies are required to measure the actin binding and nucleotide exchange activities of TgPRF using *T. gondii* actin, to ensure that the slower nucleotide exchange activity and low actin-binding affinity are not due simply to high structural divergence between vertebrate and *T. gondii* actin.

By comparing the structure of TgPRF to well-characterized eukaryotic profilins, such as ScPRF, we have identified divergent properties of TgPRF that may have implications for the function of TgPRF in parasite actin regulation. The structure of bovine profilin bound to bovine actin and extensive mutagenesis studies of yeast profilins have defined the conserved actin-binding surface of these profilins.[16,34] Twelve profilin residues are needed for actin binding in yeast. Six putative TgPRF actin-binding residues, defined by conservation to non-apicomplexan profilins, lie on the homologous yeast actin-binding protein surface, supporting the characterization of TgPRF as a true profilin. However, α-helix 3 and two residues that are known to bind actin in non-apicomplexan profilins are absent in the TgPRF and PfPRF structures. The extended β-hairpin of TgPRF may contact native *T. gondii* actin and compensate for low conservation of actin-binding residues in TgPRF. These differences suggest that TgPRF may have specialized functions compared to non-apicomplexan profilins.

The electrostatic surface potentials were calculated for TgPRF and ScPRF and mapped to the respective molecular surfaces (Fig. 6).[37,43] TgPRF shows much stronger polarity in overall surface potential

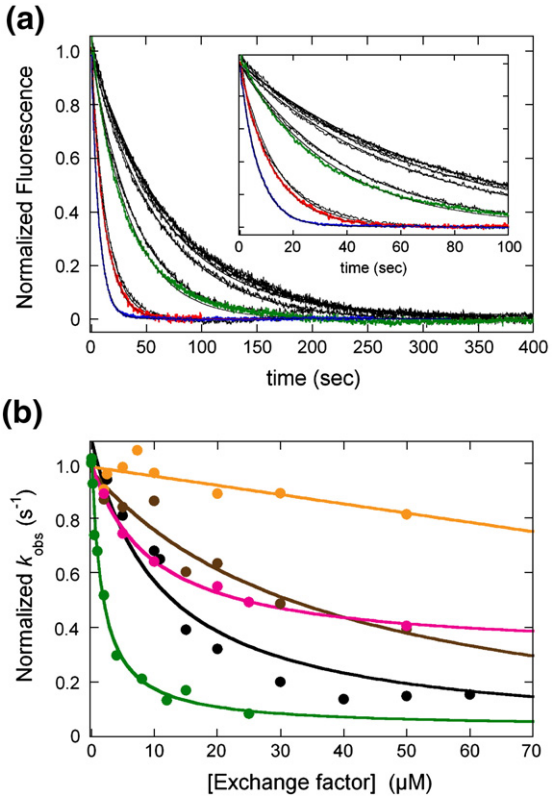

Fig. 5. Effect of TgPRF on the rate of nucleotide exchange of ATP bound monomeric actin. (a) Time courses of ε-ATP exchange from actin monomers in the absence (red trace) and presence of TgPRF (black traces; 10–60 μM from left to right. The continuous lines through the data represent the best fits to single exponentials. The final concentrations were 0.5 μM monomeric actin, 2.5 μM εATP, 2 mM ATP, and 10–60 μM TgPRF. Shown for comparison are the effects of 1.7 μM human profilin (HuPfn, blue trace) and 1.1 μM human cofilin I (green trace). The inset shows the same data and fits over shorter timescale for visualization. (b) TgPRF concentration dependence of the observed ATP exchange rate constant (black). The ε-ATP exchange rate constant of actin alone varied from 0.03 to 0.1 s^{-1} for various preparations. For comparison, the following are shown: TgPRF β-hairpin deletion mutant (ΔBH, orange), TgPRF acidic loop deletion mutant (ΔAL, pink), TgPRF point mutant 6 PM (brown), and human cofilin (green). The lines represent the best fits of the data to Eq. (1) (see Materials and Methods), which yields $K_p = 13.9 \pm 5.0$ μM for wild-type TgPRF.

compared to ScPRF. The putative actin-binding surface of TgPRF has a positive electrostatic potential with a positively charged pocket formed by the surface of β-sheet strands 7 and 8 (residues R97, K144, and R148). In contrast, the opposite face of the molecule has a negative potential.

Some profilins can bind some phosphatidylinositide lipids.[32,44] We tested TgPRF binding to phosphatidylinositol 4,5-bisphosphate (PIP2) using a liposome binding assay. TgPRF did not bind PIP2 while >90% of ScPRF bound PIP2-containing liposomes (Fig. S2). We also tested TgPRF binding to a range of phospholipids and phospholipid head group derivatives immobilized on a hydrophobic membrane. TgPRF did not bind any of the phospholipids tested using the experimental conditions described. A structure of TgPRF determined from crystals soaked in 2.5 mM of various soluble phosphatidylinositide lipid derivatives (see Materials and Methods) did not reveal any electron density corresponding to the lipid derivative.

Discussion

We have shown here that the structural features and biological activities of TgPRF diverge from those of yeast and vertebrate profilins and from a subset of the biological activities of PfPRF. We demonstrate that TgPRF slows actin nucleotide exchange on heterologous actin rather than accelerating it as do other characterized profilins, suggesting that profilin may serve distinct functions in *T. gondii* compared to other organisms. TgPRF along with other proteins such as TgADF, which promotes actin filament turnover via weak severing of filaments and strong sequestering of actin monomers,[20] may contribute to the atypical actin dynamics and short length and instability of actin filaments observed in apicomplexan protozoan parasites.

TgPRF did not bind to common phosphatidylinositide lipids immobilized on a hydrophobic membrane or to PIP2-containing liposomes (Fig. S2). In *Acanthamoeba*, there are two isoforms of profilin that differ in their binding affinity for PIP2 but not actin. The acidic isoform, profilin-I, has a 50-fold lower affinity (500 μM K_d) for PIP2 compared to the more basic profilin-II, implying that profilin-II is primarily membrane associated while profilin-I remains primarily cytoplasmic.[23] Like *Acanthamoeba* profilin-I, TgPRF may have very low affinity for phosphatidylinositide lipids. More sensitive assays are required to determine whether TgPRF binds any phosphatidylinositide lipids with a physiologically relevant dissociation constant. Binding of TgPRF to a proline-rich peptide from TgFRM2 could not be detected by ITC. TgPRF may bind to other proline-rich sequences, however, and like human profilin,[35] TgPRF may have a higher affinity for proline-rich peptides when it is bound to actin monomers. In the context of the specialized nature of the apicomplexan actin machinery, our results suggest that TgPRF may perform currently unknown functions in the parasite in addition to the activities usually assigned to profilins.

With respect to immune recognition of TgPRF, we show that stimulation of IL-12 secretion by TgPRF is dependent on TLR11. Through structure-based mutagenesis studies, we have identified the

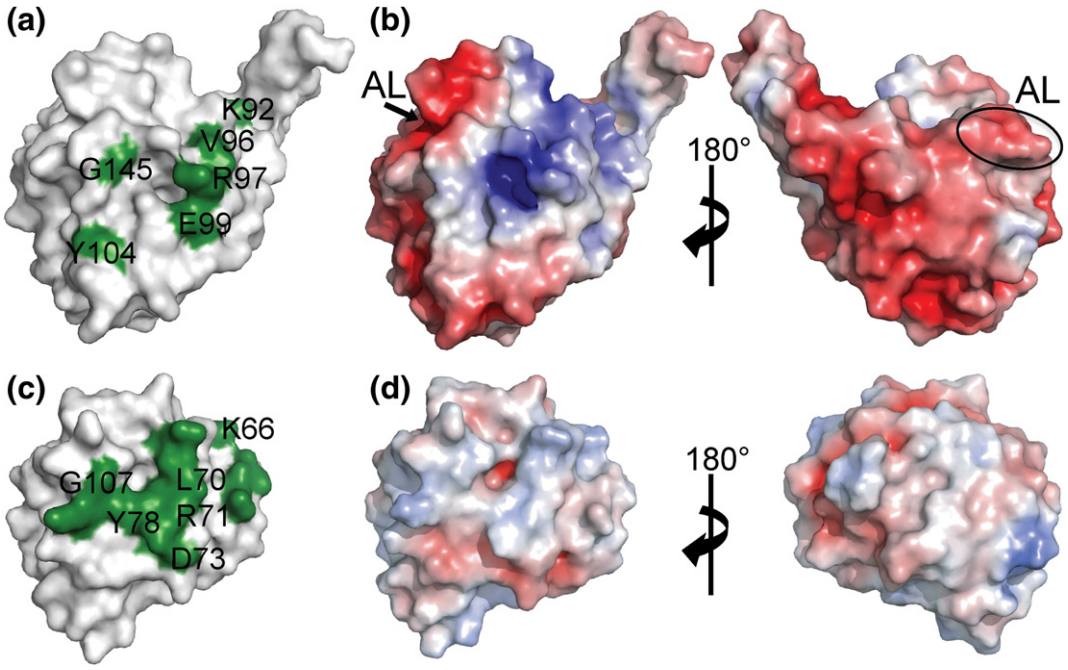

Fig. 6. Surface representations of profilins from *T. gondii* and *S. cerevisiae*. Comparison of the surface representations of TgPRF (top row) to ScPRF (bottom row) suggests divergent profilin function. (a) TgPRF residues that are conserved with known actin-binding residues in *S. cerevisiae*, *S. pombe*, and *Bos taurus* profilins are shown in green and labeled. (b) ScPRF residues known to bind actin monomers are shown in green. Only residues that share conservation with putative TgPRF actin-binding residues are labeled. (c) Comparison of electrostatic surface charge shows polarization of the TgPRF surface. (d) In comparison, the surface of *S. cerevisiae* is more uniformly neutral. Positive and negative electrostatic protein surface potentials, contoured from +5 kT to −5 kT, are shown in blue and red, respectively. The TgPRF acidic loop (AL) is labeled for reference.

parasite-specific, surface-exposed motif in TgPRF consisting of an acidic loop and a β-hairpin as the key pattern recognized by TLR11. Since changing the sequence of the β-hairpin and deletion of only the β-hairpin did not significantly affect the ability of wild-type macrophages to produce IL-12, the β-hairpin may not be as important for binding to TLR11. However, when both the acidic loop and the β-hairpin are deleted, IL-12 production is almost completely abrogated, confirming the importance of the motif in recognition by TLR11. Furthermore, by inserting the *T. gondii* recognition motif into ScPRF, we showed that the motif was sufficient to generate comparable levels of TLR11-dependent IL-12 production as TgPRF.

In a finer analysis of the role of the acidic loop in TLR11 recognition, we show that TgPRF still elicits TLR11-dependent signaling when the acidic loop is substituted with the homologous loops from *C. parvum* or *P. falciparum* but not *S. cerevisiae*. The *C. parvum* profilin acidic loop has the sequence DQGD instead of DDDD in TgPRF. This double point mutation did not significantly affect IL-12 levels after stimulation. Like TgPRF, PfPRF has four negatively charged amino acids in the acidic loop; however, it also has five additional residues that could occlude some of the acidic residues or dilute their local concentration. This may explain why substitution of the *P. falciparum* acidic loop into TgPRF results in lower levels of IL-12 production compared to wild-type TgPRF. In other apicomplexan parasites including *Plasmodium knowlesi*, *Theileria parva*, and *Babesia bovis*, the homologous acidic loops contain four to nine neutral or acidic residues. However, none of the loops are as acidic as the TgPRF sequence. Further work is necessary to determine to what extent TLR11 can recognize the acidic loops of profilins from other apicomplexan parasites and whether recognition requires other interaction partners.

Actin nucleotide exchange analysis of the TgPRF mutants suggests that the β-hairpin plays a role in actin binding since the TgPRF β-hairpin deletion mutant binds vertebrate ATP-actin only weakly. This is consistent with the model of *P. falciparum* actin bound to PfPRF proposed by Kursula *et al.*, in which negatively charged residues at the end of the β-hairpin contact positively charged actin surface residues.[32] The β-hairpin may have evolved as a novel actin-binding motif, making it indispensible. Given the diversity of length and sequence in acidic loops, it is less clear why they are retained in apicomplexan parasites. There is currently no biochemical evidence for a specific function of the

profilin acidic loop or for the analogous protein surface in any profilin characterized to date.

Our studies provide new molecular insight into the critical ability of the innate system to sense non-self molecules. TLR5 recognizes a highly conserved surface on bacterial flagellin.[45] A recent study shows that this surface includes a β-hairpin structure similar in length to the β-hairpin of TgPRF.[46] Similarly, our data suggest that TLR11 recognizes a surface motif that includes the acidic loop and the β-hairpin in apicomplexan profilins. Furthermore, differences in the acidic loop and β-hairpin across apicomplexan species appear to modulate the TLR11 response. Compounds targeting this parasite-specific protein surface could potentially provide a highly selective therapy for important human diseases such as toxoplasmosis and malaria.

Materials and Methods

Protein expression and purification

TgPRF was expressed in B834(DE3)pLysS *E. coli* cells using the pET28b vector (Novagen), in methionine-free minimal media (50% Luria broth and 50% DLM medium).[47] At mid-log growth, cells were centrifuged and the pellet was washed once with phosphate-buffered saline (PBS). Cells were then resuspended in 100% DLM medium supplemented with 2 mg/l thiamine, 0.1 μM $CaCl_2$, and 50 mg/l L-selenomethionine. Cells were induced with after 3 h of growth and grown for 15–18 h at 37 °C. Mass spectrometry of the selenomethionine-substituted protein showed that the level of selenium substitution was essentially 100% (data not shown). Selenomethionine-substituted TgPRF yield was approximately 10 mg per liter of cell culture.

Selenomethionine-substituted TgPRF was purified by nickel-affinity, anion-exchange, and size-exclusion chromatography. Cells were lysed on ice in lysis buffer [50 mM Hepes, pH 7.5, 100 mM KCl, 5% glycerol, and 10 mM DTT plus protease inhibitors (Roche)]. Cell debris were pelleted for 1.5 h at 40 krpm at 4 °C. The cell supernatant was diluted using lysis buffer without DTT to a final concentration of 1 mM DTT and purified using a HisTrap HP nickel-affinity column (GE Healthcare). TgPRF was eluted with lysis buffer and 0.25 M imidazole, pH 7.5. Protein was then dialyzed overnight in 20 mM Tris–HCl, pH 8.5, at 4 °C, 30 mM KCl, 2.5 mM $CaCl_2$, and 10 mM tris (2-carboxyethyl)phosphine with bovine α-thrombin (Haematologic Technologies) at 100 U/mg TgPRF. Uncleaved protein was retained on Ni-NTA agarose (Qiagen), and the flow-through solution was loaded on a MonoQ anion-exchange column (GE Healthcare) and eluted in a gradient to 20 mM Tris–HCl, pH 8.5, 1.0 M KCl, and 10 mM DTT. Protein was further purified on a Superdex 200 size-exclusion column (GE Healthcare) in the final protein buffer, 10 mM Tris–HCl pH 7.5, 40 mM KCl, and 10 mM DTT for crystallization, and 10 mM Hepes, pH 7.5, 100 mM KCl, and 2 mM DTT for activity assays. All TgPRF mutants were purified as described above but without the anion-exchange step.

The ScPRF mutants with *T. gondii* acidic loop and/or β-hairpin were generated from a synthetic expression construct with codons optimized for *E. coli* (Genescript). The construct included the TgPRF acidic loop and β-hairpin with flanking SpeI and PstI restriction enzyme sites, respectively. The TgPRF acidic loop (DDDD) was inserted between *S. cerevisiae* residues 32 and 33. The TgPRF β-hairpin (HEEDTIGEDGNACGKVSI) was inserted between *S. cerevisiae* residues 38 and 39. The plasmid was digested with either SpeI or PstI and religated to generate the single insertion mutants. To generate the native ScPRF, we sequentially digested the plasmid with SpeI and PstI to remove both acidic loop and β-hairpin sequence insertions. ScPRF and the three TgPRF-insertion mutants were expressed and purified as described for TgPRF mutant proteins. The acidic loop and β-hairpin peptide [acetyl]-ADDDDGWSKLYKDDHEEDTIGEDGNACGKVSI-[OH] was synthesized and judged to be greater than 98% pure by HPLC (Tufts University Core Facility).

For insect cell-expressed protein, the gene encoding TgPRF was sub-cloned into pFastBac HTb (Invitrogen). Recombinant virus was produced as described in the Invitrogen baculovirus expression system manual. Sf9 cells (Invitrogen) were infected with approximately five virus particles per cell. After 72 h, whole cells were collected by centrifugation at 300 *g* and washed once with PBS. Protein was purified as described above for *E. coli*-derived TgPRF except that tobacco etch virus protease was used to remove the N-terminal histidine tag. Typical yields were 60 mg per liter of cell culture. Mass spectrometry of TgPRF purified from *E. coli* and TgPRF purified from insect cells gave the expected molecular mass ±0.8 Da, indicating that neither protein had posttranslational modifications.

Actin was purified from rabbit back and leg skeletal muscle,[48] gel filtered over Superdex S300 in Buffer A (2 mM Tris, pH 8.0, 0.2 mM ATP, 0.5 mM DTT, 0.1 mM $CaCl_2$, and 1 mM NaN_3), and used within 1 week. Actin concentrations were determined by measuring absorbance at 290 nm using an extinction coefficient of 2.65×10^4 M^{-1} cm^{-1}.[49] Actin monomers with bound Mg-εATP were prepared by exchanging bound Ca^{2+} for Mg^{2+} with the addition of 0.2 mM ethylene glycol bis(β-aminoethyl ether)*N*,*N*′-tetra-acetic acid and 80 μM $MgCl_2$, removing free ATP with Dowex AGX-1 slurry (9% v/v), pelleting Dowex beads by centrifugation (14 kg for 20 s), and mixing supernatant with 200 μM εATP.[42,50]

Human profilin was a generous gift from Dr. Thomas Pollard and was purified as previously described.[51] Human cofilin I was purified as previously described.[38]

TgPRF crystallization and data collection

Crystals grew from a 15-mg/ml solution of TgPRF by hanging drop vapor diffusion. TgPRF (0.5 μl) in 10 mM Tris–HCl, pH 7.5, 40 mM KCl, and 10 mM DTT was mixed with 0.5 μl of 2.2 M ammonium sulfate, 0.1 M sodium citrate, pH 5.8, and 0.2 M K/Na tartrate at 16 °C. Only selenomethionine-substituted TgPRF produced crystals suitable for diffraction studies. Crystals with improved diffraction properties were obtained by micro-seeding and by controlled dehydration[52] in buffer containing 10% more ammonium sulfate than the precipitant buffer. Crystals were flash frozen in liquid nitrogen in dehydration buffer

containing 20% glycerol for data collection at 100 K. Without dehydration, crystals belonged to space group $P2_12_12_1$ and diffraction patterns contained additional reflections with variable spacings that were indicative of non-merohedral twinning. Dehydrated crystals belonged to space group $P1$ with four molecules in the asymmetric unit. See Table 2 for data collection statistics.

For TgFRM2-like peptide co-crystallization trials, peptide and protein were mixed at 4:1 and 1.5:1 molar ratios of peptide:protein with a final protein concentration of 8.5 mg/ml and 17.0 mg/ml, respectively. Crystallization drops with and without 10 mM $MgCl_2$ grew crystals as described above. For phosphatidylinositide lipid derivatives, TgPRF crystals were soaked in dehydration buffer containing 2.5 mM or 5:1 molar ratio phosphatidylinositide lipid derivative to protein with and without 10 mM $MgCl_2$. Phosphatidylinositide lipid derivatives were as follows: PIP2 C-6, inositol-1,4,5-triphosphate, inositol-1,5-diphosphate, and phosphatidylinositol-3-monophosphate C-8 (Cayman Chemicals).

Structure determination of TgPRF

The structure of TgPRF was determined by molecular replacement using PfPRF [Protein Data Bank (PDB) ID: 2JKF][32] as the search model. Phaser[53] was used to find all four molecules in the asymmetric unit. Cycles of model building with Coot[54] and positional and *B*-factor refinement with CNS[55] were performed, with non-crystallographic symmetry restraints applied to all four molecules during initial rounds of refinement. Rigid-body motions of the four TgPRF molecules in the crystal were then modeled with REFMAC5 in terms of TLS tensors for translation, libration, and correlations of libration and translation.[56] After refinement, R_{work} and R_{free} were 15.8% and 19.2%, respectively. Of all the residues, 91.3% are in the most favored regions of the Ramachandran plot, and no residues are in disallowed regions. See Table 2 for additional refinement statistics.

Table 2. Data collection and refinement statistics

Data collection	
Space group	$P1$
Cell dimensions	
a, *b*, *c* (Å)	49.53, 53.34, 68.62
α, β, γ (°)	74.70, 73.82, 68.98
Resolution (Å)[a]	40.0–1.7 (1.76–1.70)
R_{sym} or R_{merge}[a]	0.073 (0.410)
I/σ[a]	17.18 (3.0)
Completeness (%)[a]	94.0 (69.9)
Redundancy[a]	3.8 (3.5)
Number of unique reflections measured	64,017
Refinement	
Resolution (Å)	26.3–1.70
Number of reflections, working set	61,203
Number of reflections, test set	2814
R_{work}, R_{free}[b]	0.159, 0.196
Number of atoms	5841
Protein	5036
Water	753
DTT and SO_4^{2-}	52
Average *B*-factors (residual after TLS refinement)[c]	26.26 (19.0)
Protein (Å^2)	25.7 (17.1)
Water (Å^2)	28.9 (N.A.)
DTT and SO_4^{2-}	40.1 (N.A.)
RMSDs	
Bond lengths (Å)	0.01
Bond angles (°)	1.17

[a] Values for the highest-resolution shell (1.76–1.70 Å) are shown in parentheses.
[b] R_{free}, R_{work} with 5% of F_{obs} sequestered before refinement.
[c] See PDB entry 3NEC for TLS refinement parameters.

Structure comparisons, normal mode analysis, and coordinate deposition

Protein superpositions were done in CCP4,[57,58] and coordinates were viewed using PyMOL.[59] The following structures were used: PfPRF (PDB ID: 2JKF), [32] ScPRF (PDB ID: 1YPR), [60] and bovine profilin in complex with β-actin (PDB ID: 2BTF).[61] TgPRF and PfPRF are 42% identical. Protein electrostatic surface potential calculations were done using the PyMOL plugin APBS.[62] Normal mode analysis of the β-hairpin was performed with the web-based server ElNemo.[63]

Phospholipid and TgFRM2 peptide binding assays

PIP strips (Echelon Biosciences) were used to test TgPRF phospholipid binding specificity. Strips were blocked for 24 h in 5% nonfat dry milk with or without 50 μg/ml bovine serum albumin in PBS at 4 °C and then incubated in PBS with 20 μg/ml TgPRF and 50 μg/ml bovine serum albumin for 2 h. The strip was washed three times for 10 min with PBST (PBS with 0.2% Tween-20). For detection, the strip was incubated with goat anti-TgPRF antibodies (R&D Systems) at 1:30,000 dilution for 1 h followed by secondary anti-goat horseradish-peroxidase-conjugated antibodies (Abcam) at 1:50,000 dilution and developed using the ECL Advance kit (GE Healthcare). All steps were performed at 25 °C unless otherwise specified.

POPC (1-palmitoyl-2-oleoyl-*sn*-glycero-3-phosphocholine) (Avanti Polar Lipids) liposomes prepared with and without PIP2 (Cayman Chemical Company) as previously described.[64] For PIP2 liposomes, the molar ratio of POPC: PIP2 was 50:50. TgPRF or ScPRF protein was incubated for 30 min at 25 °C with liposome buffer, PC liposomes, or PIP2 liposomes at 250:1 molar ratio of PIP2 to protein. The final protein concentration for all reactions was 0.46 μM. To detect binding, we adapted a protocol from Haarer *et al.*[24] Briefly, the reactions were centrifuged using polyethersulfone micro concentrators (with 100 kDa molecular mass cutoff; Vivascience) for 5 min at 2000 krpm. Liposomes were retained and the unbound protein flow through was analyzed by SDS-PAGE. Protein bands were visualized by silver staining.

The TgFRM2-like peptide sequence was derived from TgFRM2 GeneID 20.m03963† amino acids 3402 to 3412. The peptide [acetyl]-MPPPPPPGKTP-[amide] was synthesized and judged to be greater than 98% pure by HPLC (Tufts University Core Facility). For ITC binding affinity measurements, 112 μM TgPRF was titrated with 1.68 μM peptide dissolved in TgPRF buffer at 25 °C in the

† www.toxoDB.org

calorimeter (MicroCal iTC200). Data were viewed and analyzed using the Microcal Origin software package.

TgPRF site-directed mutagenesis

TgPRF deletion mutants and chimeras were generated from the wild-type sequence by PCR using the following primers: ΔAL cttgtacaggccgcccgccgcggcgaacacaacaccgtc, gccgcggcgggcggcctgtacaaggatgatcatgaggaggac; ΔBH ggaggcctcgttatcatccttgtacagcttggaccatcc, gtacaaggatgataacgaggcctccacgatcaaagctgcag; ΔALBH primers are the same as for ΔAL and ΔBH; 2 PM and 6 PM gaagtacaaggttgtcaacattgagaaaggattcgag, ctcgaatcctttctcaatgttgacaaccttgtacttc, ggcggccagaagtaccagtttgtcaacattgagaaagg, cctttctcaatgttgacaaactggtacttctggccgcc, gcaccttcgacatcgctacgtgtgcacggtccaaggg, cccttggaccgtgcacacgtagcgatgtcgaaggtgc; TgPRF +Cp AL gccgcggcggctgatcagggtgacggatggtccaag, cttggaccatccgtcaccctgatcagccgccgcggc; TgPRF +Pf AL ccatttatcaaaatttgggtcactctcttcaccctgagccgccgcggcgaacac, cagggtgaagagagtgacccaaattttgataaatggtccaagctgtacaaggat; TgPRF +Pf BH cgttttggtagttttagtaccattttcatcttcaacttcaatatcataatcatccttgtacagctt, tatgatattgaagttgaagatgaaaatggtactaaaactaccaaaacgatcaacgaggcctccacg. TgPRF mutants were expressed in *E. coli* strain BL21(DE3) grown in Luria broth and purified as described above for wild-type protein.

CD spectroscopy

CD data were recorded on an AVIV model 215 CD spectrophotometer (AVIV Instruments) equipped with a thermoelectric temperature controller. Measurements were performed in 10 mM Hepes, pH 7.5, 100 mM KCl, and 2 mM DTT using a 1-mm-path-length quartz cuvette. Far-UV wavelength scans were recorded at 25 °C using 10 μM protein. Thermal unfolding experiments (4–95 °C) were preformed at 15–20 μM protein concentration by measuring ellipticity at 220 nm, allowing 60 s equilibration per 1 °C temperature increment. Melting temperature (T_m) for each protein was taken as the slope minimum for the first derivative of the melting curve (Table 1).

TLR11-dependent IL-12 stimulation

All experimental animals used in this study, TLR11$^{-/-}$ and wild-type littermates strains (both on C57/B6 background) were females, 6–8 weeks old, bred, and maintained in specific pathogen-free conditions. Peritoneal macrophages were isolated from mice injected intraperitoneally with 2 ml of 4% thioglycolate. After 5 days, mice were euthanized and their peritoneal cavities were lavaged with PBS. The PBS solution was harvested by syringe, centrifuged for 5 min at 1500 rpm, and resuspended into Dulbecco's modified Eagle's medium with 5% fetal bovine serum. For ELISA analysis, peritoneal macrophages were plated at 5×10^4 cells per well on a 96-well plate. Cells were stimulated with 3.0 μg/ml of TgPRF or mutant, or 5 μM CpG for 24 h at 25 °C. Supernatant was harvested and analyzed for production of IL-12(p40) by ELISA according to the manufacturer's instructions (R&D Systems). The sequence of DNA oligonucleotide CpG1826 is TCCATGACGTTCCTGACGTT.

Actin nucleotide exchange

Nucleotide exchange was measured by rapidly mixing εATP-actin monomers (1–1.5 μM) with an equilibrated mixture of 2 mM ATP and varying concentrations of TgPRF, human profilin,[51] or human cofilin[38] using an Applied Photosystems SX18 MV-R stopped-flow apparatus. Reaction experimental conditions were 10 mM Tris (pH 8.0), 45 mM KCl, 1 mM ethylene glycol bis(β-aminoethyl ether)*N*,*N*′-tetraacetic acid, 1 mM $MgCl_2$, and 5 mM DTT, at 25 °C. Time courses of fluorescence change were fitted to single exponentials. The affinity of profilin for Mg-εATP-actin monomers (K_p, expressed as a dissociation equilibrium constant), the rate constant of Mg-εATP dissociation from actin monomers (k_{-A}), and the rate constant of εATP dissociation from profilin–actin (k_{-PA}) were determined from the profilin concentration dependence of the observed nucleotide exchange rate constants (k_{obs}) as defined by Eq. (1):

$$k_{obs} = \frac{K_p k_{-A} + [P]k_{-PA}}{[P] + K_p} \quad (1)$$

Accession number

TgPRF coordinates and experimental amplitudes have been deposited in the PDB under accession code 3NEC.

Supplementary materials related to this article can be found online at doi:10.1016/j.jmb.2010.09.022

Acknowledgements

We thank Tom Pollard for comments and for his generous gift of purified human profilin. This work was supported by a Burroughs Wellcome Investigator Award to Y.M., a National Science Foundation Graduate Research fellowship to K.K., award GM071688 from the National Institutes of Health (NIH) and American Heart Association Established Investigator Award 0940075N to E.M. D.L.C., and NIH grants AI033443 and AI059440 to A.K. and S.G. E.M.D.L.C. is a National Science Foundation-CAREER Award recipient (MCB-0546353) and Hellman Family Fellow. We thank Raj Kanagalaghatta and other staff at the Northeastern Collaborative Access Team beamlines of the Advanced Photon Source, supported by award RR-15301 from the NIH National Center for Research Resources. We thank Annie Héroux and other staff at the X25 and X29A beamlines of the National Synchrotron Light Source at Brookhaven National Laboratory. Use of Advanced Photon Source (under Contract DE-AC02-06CH11357) and National Synchrotron Light Source is supported by the Offices of Biological and of Basic Energy Sciences of the U.S. Department of Energy.

References

1. Montoya, J. G. & Liesenfeld, O. (2004). Toxoplasmosis. *Lancet*, **363**, 1965–1976.
2. Dobrowolski, J. M. & Sibley, L. D. (1996). Toxoplasma invasion of mammalian cells is powered by the actin cytoskeleton of the parasite. *Cell*, **84**, 933–939.
3. Sahoo, N., Beatty, W., Heuser, J., Sept, D. & Sibley, L. D. (2006). Unusual kinetic and structural properties control rapid assembly and turnover of actin in the parasite *Toxoplasma gondii*. *Mol. Biol. Cell*, **17**, 895–906.
4. Schmitz, S., Grainger, M., Howell, S., Calder, L. J., Gaeb, M., Pinder, J. C. *et al.* (2005). Malaria parasite actin filaments are very short. *J. Mol. Biol.* **349**, 113–125.
5. Schuler, H., Mueller, A. K. & Matuschewski, K. (2005). Unusual properties of *Plasmodium falciparum* actin: new insights into microfilament dynamics of apicomplexan parasites. *FEBS Lett.* **579**, 655–660.
6. Meissner, M., Schluter, D. & Soldati, D. (2002). Role of *Toxoplasma gondii* myosin A in powering parasite gliding and host cell invasion. *Science*, **298**, 837–840.
7. Herm-Gotz, A., Delbac, F., Weiss, S., Nyitrai, M., Stratmann, R., Tomavo, S. *et al.* (2006). Functional and biophysical analyses of the class XIV *Toxoplasma gondii* myosin D. *J. Muscle Res. Cell Motil.* **27**, 139–151.
8. Dobrowolski, J. M., Niesman, I. R. & Sibley, L. D. (1997). Actin in the parasite *Toxoplasma gondii* is encoded by a single copy gene, ACT1 and exists primarily in a globular form. *Cell Motil. Cytoskeleton*, **37**, 253–262.
9. Gordon, J. L. & Sibley, L. D. (2005). Comparative genome analysis reveals a conserved family of actin-like proteins in apicomplexan parasites. *BMC Genomics*, **6**, 179.
10. Plattner, F., Yarovinsky, F., Romero, S., Didry, D., Carlier, M. F., Sher, A. & Soldati-Favre, D. (2008). *Toxoplasma* profilin is essential for host cell invasion and TLR11-dependent induction of an interleukin-12 response. *Cell Host Microbe*, **3**, 77–87.
11. Wetzel, D. M., Schmidt, J., Kuhlenschmidt, M. S., Dubey, J. P. & Sibley, L. D. (2005). Gliding motility leads to active cellular invasion by *Cryptosporidium parvum* sporozoites. *Infect. Immun.* **73**, 5379–5387.
12. Wetzel, D. M., Hakansson, S., Hu, K., Roos, D. & Sibley, L. D. (2003). Actin filament polymerization regulates gliding motility by apicomplexan parasites. *Mol. Biol. Cell*, **14**, 396–406.
13. Shaw, M. K. & Tilney, L. G. (1999). Induction of an acrosomal process in *Toxoplasma gondii*: visualization of actin filaments in a protozoan parasite. *Proc. Natl Acad. Sci. USA*, **96**, 9095–9099.
14. Ryning, F. W. & Remington, J. S. (1978). Effect of cytochalasin D on *Toxoplasma gondii* cell entry. *Infect. Immun.* **20**, 739–743.
15. Pollard, T. D., Blanchoin, L. & Mullins, R. D. (2000). Molecular mechanisms controlling actin filament dynamics in nonmuscle cells. *Annu. Rev. Biophys. Biomol. Struct.* **29**, 545–576.
16. Schutt, C. E., Myslik, J. C., Rozycki, M. D., Goonesekere, N. C. & Lindberg, U. (1993). The structure of crystalline profilin-beta-actin. *Nature*, **365**, 810–816.
17. Schuler, H., Mueller, A. K. & Matuschewski, K. (2005). A *Plasmodium* actin-depolymerizing factor that binds exclusively to actin monomers. *Mol. Biol. Cell*, **16**, 4013–4023.
18. Nishida, E. (1985). Opposite effects of cofilin and profilin from porcine brain on rate of exchange of actin-bound adenosine 5′-triphosphate. *Biochemistry*, **24**, 1160–1164.
19. Blanchoin, L. & Pollard, T. D. (1998). Interaction of actin monomers with *Acanthamoeba* actophorin (ADF/cofilin) and profilin. *J. Biol. Chem.* **273**, 25106–25111.
20. Mehta, S. & Sibley, L. D. (2010). *Toxoplasma gondii* actin depolymerizing factor acts primarily to sequester G-actin. *J. Biol. Chem.* **285**, 6835–6847.
21. Schuler, H. & Matuschewski, K. (2006). Regulation of apicomplexan microfilament dynamics by a minimal set of actin-binding proteins. *Traffic*, **7**, 1433–1439.
22. Baum, J., Tonkin, C. J., Paul, A. S., Rug, M., Smith, B. J., Gould, S. B. *et al.* (2008). A malaria parasite formin regulates actin polymerization and localizes to the parasite–erythrocyte moving junction during invasion. *Cell Host Microbe*, **3**, 188–198.
23. Machesky, L. M., Goldschmidt-Clermont, P. J. & Pollard, T. D. (1990). The affinities of human platelet and *Acanthamoeba* profilin isoforms for polyphosphoinositides account for their relative abilities to inhibit phospholipase C. *Cell Regul.* **1**, 937–950.
24. Haarer, B. K., Petzold, A. S. & Brown, S. S. (1993). Mutational analysis of yeast profilin. *Mol. Cell. Biol.* **13**, 7864–7873.
25. Lassing, I. & Lindberg, U. (1985). Specific interaction between phosphatidylinositol 4,5-bisphosphate and profilactin. *Nature*, **314**, 472–474.
26. Goldschmidt-Clermont, P. J., Machesky, L. M., Baldassare, J. J. & Pollard, T. D. (1990). The actin-binding protein profilin binds to PIP2 and inhibits its hydrolysis by phospholipase C. *Science*, **247**, 1575–1578.
27. Goldschmidt-Clermont, P. J., Kim, J. W., Machesky, L. M., Rhee, S. G. & Pollard, T. D. (1991). Regulation of phospholipase C-gamma 1 by profilin and tyrosine phosphorylation. *Science*, **251**, 1231–1233.
28. Ostrander, D. B., Gorman, J. A. & Carman, G. M. (1995). Regulation of profilin localization in *Saccharomyces cerevisiae* by phosphoinositide metabolism. *J. Biol. Chem.* **270**, 27045–27050.
29. West, A. P., Koblansky, A. A. & Ghosh, S. (2006). Recognition and signaling by toll-like receptors. *Annu. Rev. Cell Dev. Biol.* **22**, 409–437.
30. Yarovinsky, F., Zhang, D., Andersen, J. F., Bannenberg, G. L., Serhan, C. N., Hayden, M. S. *et al.* (2005). TLR11 activation of dendritic cells by a protozoan profilin-like protein. *Science*, **308**, 1626–1629.
31. Rosenberg, B., Juckett, D. A., Aylsworth, C. F., Dimitrov, N. V., Ho, S. C., Judge, J. W. *et al.* (2005). Protein from intestinal *Eimeria* protozoan stimulates IL-12 release from dendritic cells, exhibits antitumor properties in vivo and is correlated with low intestinal tumorigenicity. *Int. J. Cancer*, **114**, 756–765.
32. Kursula, I., Kursula, P., Ganter, M., Panjikar, S., Matuschewski, K. & Schuler, H. (2008). Structural basis for parasite-specific functions of the divergent profilin of *Plasmodium falciparum*. *Structure*, **16**, 1638–1648.
33. Murthy, K. G., Deb, A., Goonesekera, S., Szabo, C. & Salzman, A. L. (2004). Identification of conserved domains in *Salmonella muenchen* flagellin that are essential for its ability to activate TLR5 and to induce an inflammatory response in vitro. *J. Biol. Chem.* **279**, 5667–5675.

34. Ezezika, O. C., Younger, N. S., Lu, J., Kaiser, D. A., Corbin, Z. A., Nolen, B. J. *et al.* (2009). Incompatibility with formin Cdc12p prevents human profilin from substituting for fission yeast profilin: insights from crystal structures of fission yeast profilin. *J. Biol. Chem.* **284**, 2088–2097.
35. Ferron, F., Rebowski, G., Lee, S. H. & Dominguez, R. (2007). Structural basis for the recruitment of profilin–actin complexes during filament elongation by Ena/VASP. *EMBO J.* **26**, 4597–4606.
36. Kursula, P., Kursula, I., Massimi, M., Song, Y. H., Downer, J., Stanley, W. A. *et al.* (2008). High-resolution structural analysis of mammalian profilin 2a complex formation with two physiological ligands: the formin homology 1 domain of mDia1 and the proline-rich domain of VASP. *J. Mol. Biol.* **375**, 270–290.
37. Eads, J. C., Mahoney, N. M., Vorobiev, S., Bresnick, A. R., Wen, K. K., Rubenstein, P. A. *et al.* (1998). Structure determination and characterization of *Saccharomyces cerevisiae* profilin. *Biochemistry*, **37**, 11171–11181.
38. De La Cruz, E. M. (2005). Cofilin binding to muscle and non-muscle actin filaments: isoform-dependent cooperative interactions. *J. Mol. Biol.* **346**, 557–564.
39. Hayden, S. M., Miller, P. S., Brauweiler, A. & Bamburg, J. R. (1993). Analysis of the interactions of actin depolymerizing factor with G- and F-actin. *Biochemistry*, **32**, 9994–10004.
40. Hawkins, M., Pope, B., Maciver, S. K. & Weeds, A. G. (1993). Human actin depolymerizing factor mediates a pH-sensitive destruction of actin filaments. *Biochemistry*, **32**, 9985–9993.
41. De La Cruz, E. (2009). How cofilin severs an actin filament. *Biophys. Rev.* **1**, 51–59.
42. Vinson, V. K., De La Cruz, E. M., Higgs, H. N. & Pollard, T. D. (1998). Interactions of *Acanthamoeba* profilin with actin and nucleotides bound to actin. *Biochemistry*, **37**, 10871–10880.
43. Dolinsky, T. J., Nielsen, J. E., McCammon, J. A. & Baker, N. A. (2004). PDB2PQR: an automated pipeline for the setup of Poisson–Boltzmann electrostatics calculations. *Nucleic Acids Res.* **32**, W665–667.
44. Fedorov, A. A., Magnus, K. A., Graupe, M. H., Lattman, E. E., Pollard, T. D. & Almo, S. C. (1994). X-ray structures of isoforms of the actin-binding protein profilin that differ in their affinity for phosphatidylinositol phosphates. *Proc. Natl Acad. Sci. USA*, **91**, 8636–8640.
45. Smith, K. D., Andersen-Nissen, E., Hayashi, F., Strobe, K., Bergman, M. A., Barrett, S. L. *et al.* (2003). Toll-like receptor 5 recognizes a conserved site on flagellin required for protofilament formation and bacterial motility. *Nat. Immunol.* **4**, 1247–1253.
46. de Zoete, M. R., Keestra, A. M., Wagenaar, J. A. & van Putten, J. P. (2010). Reconstitution of a functional toll-like receptor 5 binding site in *Campylobacter jejuni* flagellin. *J. Biol. Chem.* **285**, 12149–12158.
47. Coligan, J. E. (1995). *Current Protocols in Protein Science.* Wiley, New York, NY.
48. Spudich, J. A. & Watt, S. (1971). The regulation of rabbit skeletal muscle contraction. I. Biochemical studies of the interaction of the tropomyosin–troponin complex with actin and the proteolytic fragments of myosin. *J. Biol. Chem.* **246**, 4866–4871.
49. Houk, T. W., Jr & Putman, S. V. (1973). Location of the creatine phosphokinase binding site of myosin. *Biochem. Biophys. Res. Commun.* **55**, 1271–1277.
50. De La Cruz, E. M. & Pollard, T. D. (1995). Nucleotide-free actin: stabilization by sucrose and nucleotide binding kinetics. *Biochemistry*, **34**, 5452–5461.
51. Fedorov, A. A., Pollard, T. D. & Almo, S. C. (1994). Purification, characterization and crystallization of human platelet profilin expressed in *Escherichia coli*. *J. Mol. Biol.* **241**, 480–482.
52. Heras, B. & Martin, J. L. (2005). Post-crystallization treatments for improving diffraction quality of protein crystals. *Acta Crystallogr. Sect. D: Biol. Crystallogr.* **61**, 1173–1180.
53. McCoy, A. J., Grosse-Kunstleve, R. W., Adams, P. D., Winn, M. D., Storoni, L. C. & Read, R. J. (2007). Phaser crystallographic software. *J. Appl. Crystallogr.* **40**, 658–674.
54. Emsley, P. & Cowtan, K. (2004). Coot: model-building tools for molecular graphics. *Acta Crystallogr., Sect. D: Biol. Crystallogr.* **60**, 2126–2132.
55. Brunger, A. T., Adams, P. D., Clore, G. M., DeLano, W. L., Gros, P., Grosse-Kunstleve, R. W. *et al.* (1998). Crystallography & NMR system: a new software suite for macromolecular structure determination. *Acta Crystallogr. Sect. D: Biol. Crystallogr.* **54**, 905–921.
56. Winn, M. D., Isupov, M. N. & Murshudov, G. N. (2001). Use of TLS parameters to model anisotropic displacements in macromolecular refinement. *Acta Crystallogr. Sect. D: Biol. Crystallogr.* **57**, 122–133.
57. Krissinel, E. & Henrick, K. (2004). Secondary-structure matching (SSM), a new tool for fast protein structure alignment in three dimensions. *Acta Crystallogr. Sect. D: Biol. Crystallogr.* **60**, 2256–2268.
58. Collaborative Computational Project, Number 4 (1994). The CCP4 suite: programs for protein crystallography. *Acta Crystallogr. Sect. D: Biol. Crystallogr.* **50**, 760–763.
59. Delano, W. L. (2002). *The PyMOL Molecular Graphics System.* DeLano Scientific LLC, San Carlos, CA.
60. Eads, J. C., Mahoney, N. M., Vorobiev, S., Bresnick, A. R., Wen, K. K., Rubenstein, P. A. *et al.* (1998). Structure determination and characterization of *Saccharomyces cerevisiae* profilin. *Biochemistry*, **37**, 11171–11181.
61. Schutt, C. E., Myslik, J. C., Rozycki, M. D., Goonesekere, N. C. W. & Lindberg, U. (1993). The structure of crystalline profilin beta-actin. *Nature*, **365**, 810–816.
62. Baker, N. A., Sept, D., Joseph, S., Holst, M. J. & McCammon, J. A. (2001). Electrostatics of nanosystems: application to microtubules and the ribosome. *Proc. Natl Acad. Sci. USA*, **98**, 10037–10041.
63. Suhre, K. & Sanejouand, Y. H. (2004). ElNemo: a normal mode web server for protein movement analysis and the generation of templates for molecular replacement. *Nucleic Acids Res*, **32**, W610–614.
64. Kagan, J. C. & Medzhitov, R. (2006). Phosphoinositide-mediated adaptor recruitment controls Toll-like receptor signaling. *Cell*, **125**, 943–955.